JOM, Vol. 75, No. 7, 2023
https://doi.org/10.1007/s11837-023-05846-y

TECHNICAL ARTICLE

Gas-Based Direct Reduction of Hongge Vanadium Titanomagnetite Pellets with Different MgO Additions

RUIQI ZENG,[1,2] NAN WANG,[2,3,4] and WEI LI[1,2,5]

1.—Key Laboratory for Ecological Metallurgy of Multimetallic Mineral (Ministry of Education), Northeastern University, Shenyang 110819, China. 2.—School of Metallurgy, Northeastern University, Shenyang 110819, China. 3.—Institute for Frontier Technologies of Low-Carbon Steelmaking, Shenyang 110819, China. 4.—e-mail: wangn@smm.neu.edu.cn. 5.—e-mail: lw_neu@126.com

In this study, the reduction of Hongge vanadium titanomagnetite pellet (HVTMP) with different MgO additions was investigated under a simulated shaft furnace atmosphere. The HVTMP porosity was found to increase with MgO addition, which promoted the initial reduction rate; however, the final reduction degree decreased as the reduction proceeded. X-ray diffraction showed that $MgFe_2O_4$ was formed by adding MgO, and the metallic iron peak intensity weakened. The formed $MgFe_2O_4$ was embedded into Fe_2TiO_4, which prevented the further reduction of Fe_2TiO_4 or the migration of metallic iron, thereby reducing the degree of metallization. The reduction swelling decreased and the compressive strength of the reduced HVTMP increased as MgO addition increased, which was mainly attributed to an increase in its hardness. This work establishes a relationship between MgO and reduction, which could provide a useful reference regarding the effective utilization of HVTMP in shaft furnaces and promote the development of sustainable metallurgy.

INTRODUCTION

The iron and steel industry plays an essential role in supporting the sustainable development of the Chinese economy. Vanadium titanomagnetite (VTM) is a typical multimetallic mineral resource in China.[1–3] Hongge VTM (HVTM) from the Panxi region of China contains not only iron, vanadium, and titanium, but also a high chromium content. This so-called high-chromium VTM accounts for 68% of the total chromium reserves in China,[4–6] making it necessary to find an effective process to utilize this potentially valuable HVTM resource.

Previously proposed techniques for the utilization of VTM include blast furnace (BF) and coal-based direct reduction processes.[7–14] In the BF process, > 90% of titanium enters the BF slag and almost all of the iron is reduced into a hot metal. More than 70% of vanadium is contained in the pig iron, which is oxidized into vanadium slag in a converter furnace. The titanium in the BF slag is difficult to recover because of the low TiO_2 grade (only 10–25%), which wastes large quantities of titanium resources.[15] The coal-based direct reduction process has a relatively low efficiency, high energy consumption, and high operating temperature, which hinder the development of sustainable metallurgical processes.[16] Therefore, HVTM has not been put into industrial production or large-scale commercial use.

An innovative, sustainable HVTM smelting process has been proposed to increase the recovery rates of valuable elements in our laboratory.[17,18] In this method, HVTM is first pelletized and roasted. Then, the roasted HVTM pellet (HVTMP) is reduced in a gas-based shaft furnace before being melted in an electric furnace to recover iron, titanium, vanadium, and chromium. The roasted pellet has excellent metallurgical properties, uniform size, and high physical strength. The gas-based direct reduction of HVTMP is the most important step of this process.

(Received September 20, 2022; accepted April 10, 2023; published online May 2, 2023)

Many previous researchers have investigated the gas-based direct reduction of VTM and other minerals.[19–26] Zhang et al.[19] investigated the weak reduction of preoxidized Panzhihua ilmenite by hydrogen. Sun et al.[22] studied the reduction mechanism of VTM by H_2-Ar gas mixtures in a laboratory fixed bed reactor. Wang et al.[25] reduced titania-ferrous solution ore in a temperature range from 800°C to 1100°C with a 10–100 vol.% H_2-Ar gas mixture. Magnesium is an important component of HVTM and may affect its reduction behavior. However, in most previous studies, gas-based direct reduction behavior of pellet affected by MgO was not clearly evaluated. In particular, clear understanding was limited about the effect of MgO on the swelling of reduced HVTMP. Besides, similar studies on ordinary iron ores may not be applicable to the gas-based direct reduction of HVTMP, especially under a simulated shaft furnace atmosphere. Thus, as an integral part of developing a novel and clean smelting process for the comprehensive utilization of HVTM, it is worth to investigate the influence of MgO on the gas-based direct reduction of HVTMP, which could help us optimize process parameters.

The objective of the present study is to determine the effects of MgO addition on the gas-based reduction of HVTMP using shaft furnace reducing gas simulations. The reduction degree, phase composition, microstructure, reduction swelling, and compressive strength of reduced HVTMP with different MgO additions were investigated as discussed in detail below. The results of this work show a noteworthy relationship between MgO and its reduction, which could provide guidance for improving the comprehensive utilization of HVTM.

EXPERIMENTAL PROCEDURE

Materials

HVTM used in this study was obtained from Hongge mineral resources in the Panxi region of China. The chemical compositions of HVTM are provided in Table I. The total iron content is 54.54%, the TiO_2 content is 9.26%, and the Cr_2O_3 content is as high as 1.48%. The phase composition of HVTM is shown in Fig. 1. The main phases are magnetite (Fe_3O_4) and titanomagnetite ($Fe_{2.75}Ti_{0.25}O_4$). Chromium and vanadium exist in the form of chromite ($FeCr_2O_4$) and coulsonite (Fe_2VO_4). Analytically pure MgO was used as the additive.

Experimental Apparatus and Methods

Roasted HVTMP with different MgO additions was prepared in a step-wise process. The binder was bentonite, and 8.5% water was used in the disc-pelletizer process. First, HVTM and bentonite were uniformly mixed with MgO at mass ratios in the range 0–6% in increments of 2%. The mixture was pelletized into 11.5–12.5-mm green pellets in a disc pelletizer. The green pellets were dried at 105°C for 5 h in a constant temperature drying oven. The oxidation roasting of HVTMP was performed in a muffle furnace. When the muffle furnace was heated to the preheating temperature of 900°C at a constant heating rate of 10°C/min, HVTMP was placed in the constant temperature zone and held for 10 min. Subsequently, the muffle furnace was increased to the roasting temperature of 1200°C and held for 20 min. Air was introduced through the gas inlet throughout the oxidation roasting process. The roasted HVTMP was quickly removed from the muffle furnace and cooled to ambient temperature.

A gas-based shaft furnace was used for the reduction experiment (Fig. 2). The shaft furnace reactor was made of corundum, with a height of 550 mm and inner diameter of 60 mm. The system mainly consisted of a shaft furnace connected with an electric balance. The output of the electric balance was connected to a computer to continuously measure the weight of pellets as a function of time during the reduction process. The flow rate of different gases was adjusted precisely through a

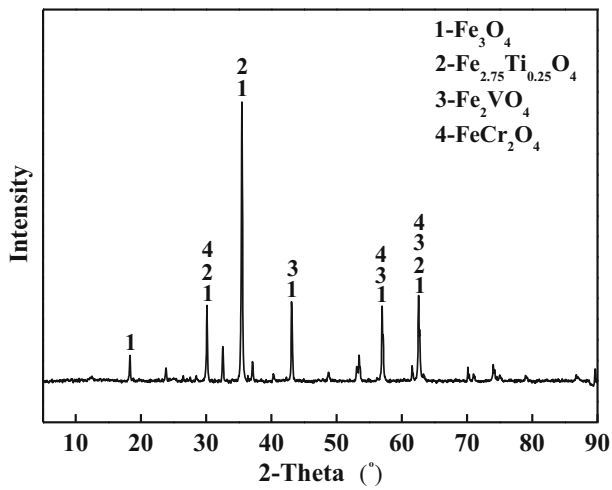

Fig. 1. XRD patterns of HVTM.

Table I. Chemical composition of HVTM (%)

TFe	FeO	CaO	SiO_2	MgO	Al_2O_3	TiO_2	V_2O_5	Cr_2O_3	S	P
54.54	26.25	0.98	4.88	2.98	2.50	9.26	0.62	1.48	0.48	0.01

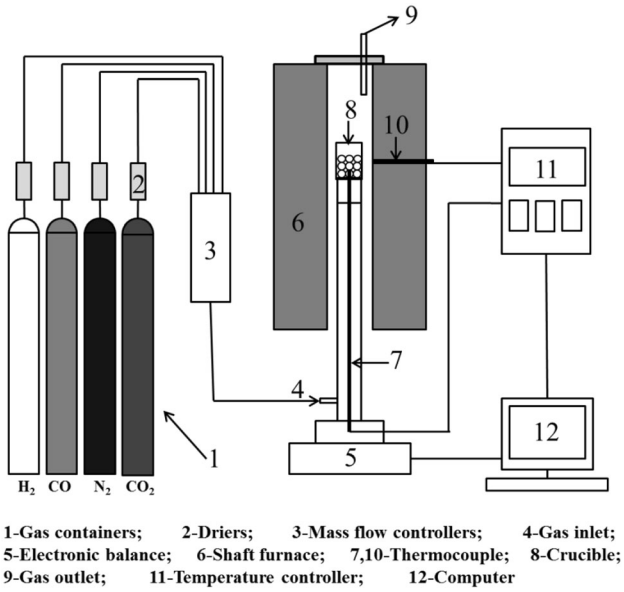

Fig. 2. Schematic diagram of shaft furnace.

mass flow controller. The actual temperature of the furnace and pellets was measured through a temperature controller. The constant zone of the furnace was measured to ensure a relatively stable (within ± 2 C) temperature. The roasted HVTMP was placed into a heat-resistant steel crucible and then into the furnace. A gas mixture of 64.3%H_2 + 25.7%CO + 5%CO_2 + 5%N_2 at a flow rate of 4 L/min was used to simulate the reduction process in a gas-based shaft furnace. The roasted HVTMP was heated to 1050°C under N_2 atmosphere, and then N_2 was switched to a reducing gas to start the reduction. The weight of the pellet was automatically measured and recorded by a computer throughout this process. The reduced HVTMP was then taken out of the furnace and cooled to room temperature under Ar protection.

The reduction degree (R) was calculated as follows:

$$R = \left[\frac{0.11w_1}{0.43w_2} + \frac{m_1 - m_t}{m_0 w_2 \times 0.43} \times 100\right] \times 100\% \quad (1)$$

where w_1 is the ferrous content in the roasted pellet, m_1 is the initial mass of the pellet after the removal of moisture, m_t is the mass of the pellet after time t, w_2 is the total iron content before reduction, m_0 is the initial mass of the pellet, 0.11 is a necessary conversion factor for the amount of oxygen required to oxidize FeO to Fe_2O_3, and 0.43 is a conversion factor for the amount of oxygen required to oxidize the total amount of Fe to Fe_2O_3.

The metallization degree was calculated as follows:

$$\text{Metallization degree} = M_{Fe}/T_{Fe} \times 100\% \quad (2)$$

where M_{Fe} is the mass fraction of metallic iron and T_{Fe} is the mass fraction of total iron after reduction.

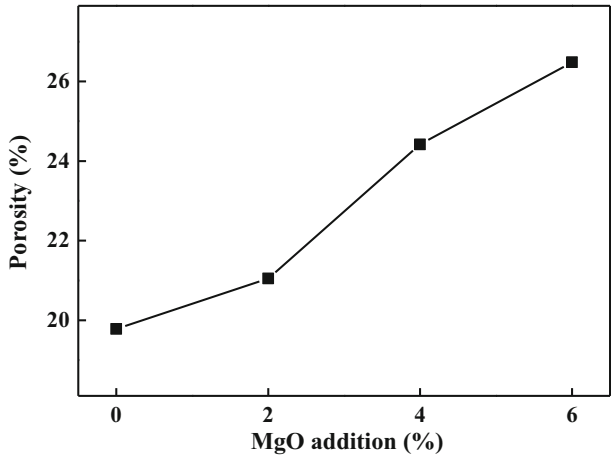

Fig. 3. Effect of MgO on the porosity of roasted HVTMP.

The reduction swelling index is an important indicator of pellet swelling behavior throughout reduction, which can be calculated as follows:

$$\text{Swelling index} = (V_a - V_0)/V_0 \times 100\% \quad (3)$$

where V_a is the volume of the reduced pellet and V_0 is the volume of the roasted pellet.

Characterization

A mercury injection apparatus (Micromeritics Instrument Corp., AutoPore-9500, USA) was used to measure the porosity of HVTMP. The porosity was measured using the following procedure: the selection of the penetrometer, low-pressure operation, high-pressure operation, and obtaining the output data. The chemical composition was analyzed by inductively coupled plasma optical emission spectrometry (ICP-OES). The Fe^{2+} content was measured by chemical titration. X-ray diffraction (XRD, PANalytical, The Netherlands) was used to characterize the phase composition of samples. The morphology was observed by scanning electron microscopy (SEM, Zeiss, Germany) combined with energy-dispersive spectroscopy (EDS). The reduction swelling and compressive strength were measured according to the standards of ISO 4689:2007 and ISO 4700, respectively. The hardness of the reduced HVTMP was analyzed on a digital microhardness tester (HVS-1000).

RESULTS AND DISCUSSION

Characterization of Roasted HVTMP

The porosity and microstructure of roasted HVTMP with different MgO additions are shown in Figs. 3 and 4, respectively. The porosity of roasted HVTMP was found to increase gradually with MgO addition. When roasted without MgO, the porosity was 19.78% and reached 21.05% upon MgO addition of 2%. The grains were in close contact and were uniformly distributed when MgO addition was

0%, with no observable pores, suggesting a homogeneous microstructure. After 4% MgO addition, the grains became loose and disordered with some separated grains and residual pores. Because of this, MgO negatively affected the induration of roasted HVTMP.

Reduction Degree

Figure 5 shows the reduction degree-time curves of HVTMP with different MgO additions. The curves suggest that HVTMP reduction was strongly affected by the addition of MgO. At the original reduction stage, MgO addition increased the reduction degree, which further increased upon continually increasing the MgO addition. This was attributed to the increased porosity of HVTMP with MgO addition, which allowed reducing gases to pass easily through the pellets. However, at a certain point in the reduction process, the final reduction degree decreased with further increase in MgO addition.

MgO addition also decreased the metallization degree of reduced HVTMP, as shown in Fig. 6. As the MgO addition increased from 0 to 2%, the metallization degree of the reduced HVTMP decreased from 91.05% to 73.26%. When the MgO addition further increased from 2% to 4%, the

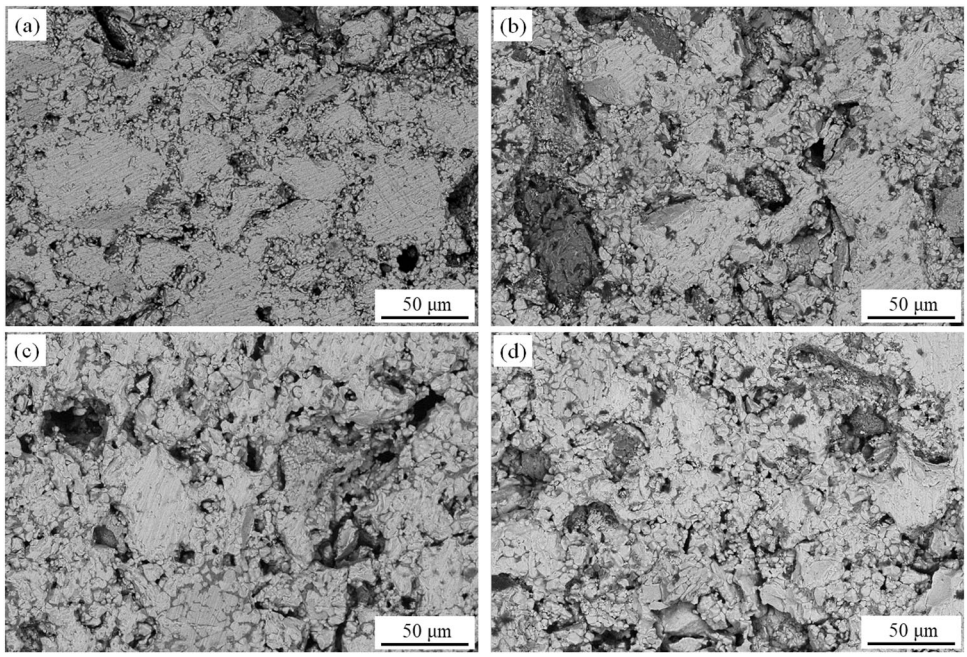

Fig. 4. Effect of MgO on the microstructure of roasted HVTMP: (a) 0%; (b) 2%; (c) 4%; (d) 6%.

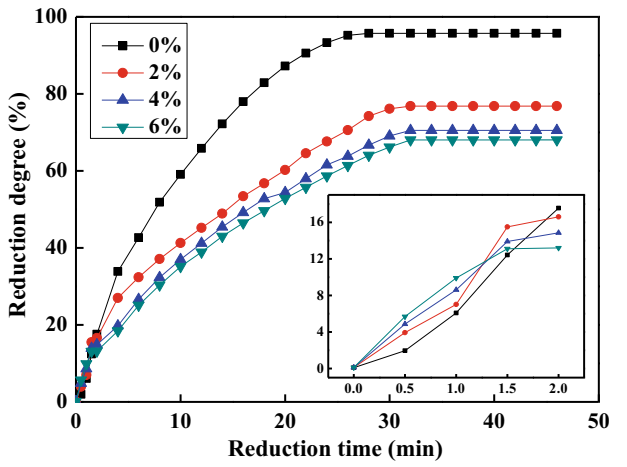

Fig. 5. Effect of MgO on the reduction degree of reduced HVTMP.

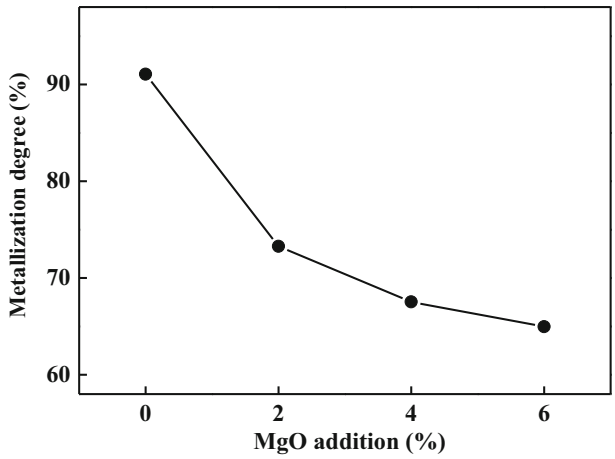

Fig. 6. Metallization degree of reduced HVTMP with different MgO additions.

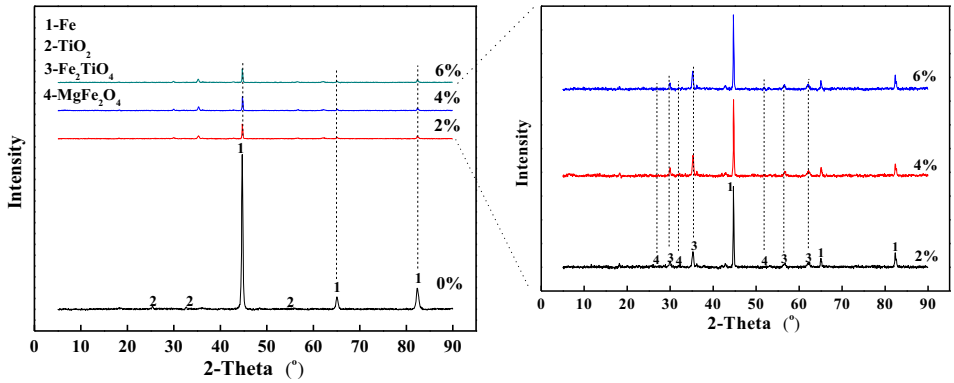

Fig. 7. Effect of MgO on the phase transformation of reduced HVTMP.

metallization degree decreased from 73.26% to 67.52%.

Phase Composition

The XRD patterns show the effects of MgO on the phase transformation of HVTMP during the reduction process (Fig. 7). The diffraction peaks of different phases changed gradually as the MgO addition increased. The main phases of reduced HVTMP without MgO addition included metallic iron and a small amount of TiO_2. When the MgO addition was 2%, the peak intensity of metallic iron was weakened and TiO_2 became undetectable as diffraction peaks of Fe_2TiO_4 and $MgFe_2O_4$ appeared.

The ionic radii of Fe^{2+} and Mg^{2+} are similar, allowing Mg^{2+} to easily enter the magnetite lattice to form $MgFe_2O_4$ by displacing Fe^{2+} ions. Mg^{2+} and Fe^{2+} can also replace each other to form a completely continuous (Fe, Mg)O solid solution. When MgO was added, Mg^{2+} diffused into the magnetite lattice, replaced Fe^{2+}, and formed $MgFe_2O_4$. At relatively high MgO additions, the peak intensities of metallic iron further decreased, while those of Fe_2TiO_4 and $MgFe_2O_4$ became stronger. MgO may inhibit the further reduction of Fe_2TiO_4 and therefore weaken the peak intensity of metallic iron, which was evidenced by the observed metallization degree.

Microstructure Evolution

MgO addition appears to markedly change the reduction process of HVTMP. SEM–EDS observations of this process are shown in Supplementary Fig. S1 (refer to online supplementary material). When reduced without MgO addition, the microstructure showed three distinct regions, including bright, light gray, and gray phases. The bright phase, which was identified as metallic iron, was distributed evenly and aggregated to form a large and continuous area. Gangue phases surrounded the dense metallic iron grains with clearly observable boundaries. When MgO addition was 2%, some metallic iron grains were broken from large pieces into small grains. The connection between metallic iron grains weakened, and several pores formed. The EDS of point 2 showed that magnesium titanium compounds containing unreduced iron oxide also formed and remained in the gangue phase. The XRD analysis confirmed that this phase was $MgFe_2O_4$ connected with Fe_2TiO_4. The further reduction of Fe_2TiO_4 and the diffusion and growth of metallic iron grains were prohibited, resulting in a decrease in metallization degree (though MgO did enhance the reduction degree initially).

With the increase of MgO addition, more large pores formed as the metallic iron grains further decreased in size. Only a few of them aggregated or connected with each other. The scattering of metallic iron grains became more obvious, and more Mg-rich phases were embedded into the Ti–rich phases, restricting the further reduction of Ti–rich phases. The map scanning analysis of the reduced HVTMP with 4% MgO addition is shown in Supplementary Fig. S2, where magnesium is randomly distributed with metallic iron. Thus, $MgFe_2O_4$ was not reduced during the reduction process.

Reduction Swelling and Compressive Strength

Reduction swelling and compressive strength are important performance indicators for reduced pellets. A low reduction swelling and high compressive strength are conducive to favorable gas permeability in a gas-based shaft furnace. The relationship between the reduction swelling index and compressive strength of reduced HVTMP with different MgO additions is shown in Supplementary Fig. S3. An increase in MgO addition appears to significantly decrease the reduction swelling. Without MgO addition, the reduction swelling of reduced HVTMP was 12.95% and reached a minimum of 6.92% with MgO addition of 6%. The compressive

strength of reduced HVTMP increased with the MgO addition, which was contrary to the change in reduction swelling. The reduction swelling and compressive strength showed an obvious linear correlation in Supplementary Fig. S4, as calculated by the following linear regression equation:

$$C = -27.32S + 810.04 \quad (4)$$

where C is the compressive strength and S is the reduction swelling index of the reduced HVTMP.

To analyze the mechanism whereby MgO influenced the compressive strength and reduction swelling, the hardness of the reduced HVTMP was measured on a digital micro-hardness tester. As shown in Supplementary Fig. S5, the hardness of the samples increased gradually with increase in MgO addition. The hardness was 386.5 kg/mm^2 in the absence of MgO and increased to 441.9 kg/mm^2 as MgO addition increased to 2%. Hardness reflects the extent of defects. Structural defects such as cracks readily form during the reduction of HVTMP, which decrease their hardness. MgO addition in this experiment caused hardness to increase, thus increasing the compressive strength and decreasing the reduction swelling of reduced HVTMP.

CONCLUSION

In this study, the gas-based direct reduction of HVTMP with different MgO additions was investigated under a simulated shaft furnace atmosphere. Our conclusions can be summarized as follows.

1. The reduction degree initially increased with MgO addition, which was mainly attributed to an increase in the porosity of HVTMP. However, the final reduction degree decreased because of the formation of $MgFe_2O_4$, which was difficult to reduce, and eventually inhibited the reduction process.
2. With the increase of MgO addition, more $MgFe_2O_4$ was formed and embedded into Fe_2TiO_4, which prevented the further reduction of Fe_2TiO_4. The number and size of metallic iron grains gradually decreased, and only some eventually aggregated and connected with each other, thereby decreasing the metallization degree.
3. The MgO addition significantly affected the reduction swelling and compressive strength of reduced HVTMP. With the increase of MgO, the hardness of reduced HVTMP increased, resulting in the increase of compressive strength and decrease of reduction swelling of reduced HVTMP.

SUPPLEMENTARY INFORMATION

The online version contains supplementary material available at https://doi.org/10.1007/s11837-023-05846-y.

ACKNOWLEDGEMENTS

This work is financially supported by the National Natural Science Foundation of China (51904066, 52074077, and 52274325), the Natural Science Foundation of Liaoning Province (2023-MS-075), and the Fundamental Research Funds for the Central Universities.

CONFLICT OF INTEREST

The authors declare that they have no conflict of interest.

REFERENCES

1. X.W. Lv, Z.G. Lun, J.Q. Yin, and C.G. Bai, *ISIJ Int.* 53, 1115 (2013).
2. L.Y. Shi, Y.L. Zhen, D.S. Chen, L.N. Wang, and T. Qi, *ISIJ Int.* 58, 627 (2018).
3. T. Hu, X.W. Lv, C.G. Bai, Z.G. Lun, and G.B. Qiu, *ISIJ Int.* 53, 557 (2013).
4. H.G. Du, *Principle of Smelting Vanadium-titanium Magnetite in the Blast Furnace* (Science Press, Beijing, 1996), p3.
5. H.M. Long, T.J. Chun, P. Wang, Q.M. Meng, Z.X. Di, and J.X. Li, *Metall. Mater. Trans. B* 47, 1765 (2016).
6. W.J. Huang, Y.H. Zhao, S. Yu, L.X. Zhang, Z.C. Ye, N. Wang, and M. Chen, *ISIJ Int.* 56, 594 (2016).
7. Y.Z. Wang, J.L. Zhang, Z.J. Liu, and C.B. Du, *JOM* 69, 2397 (2017).
8. Y.M. Zhang, L.Y. Yi, L.N. Wang, D.S. Chen, W.J. Wang, Y.H. Liu, H.X. Zhao, and T. Qi, *Int. J. Miner. Metall. Mater.* 24, 504 (2017).
9. F.Q. Zheng, G.Z. Qiu, Y.F. Guo, F. Chen, S. Wang, and T. Jiang, *ISIJ Int.* 57, 1767 (2017).
10. H.P. Gou, G.H. Zhang, X. Yuan, and K.C. Chou, *ISIJ Int.* 56, 744 (2016).
11. E.H. Wu, R. Zhu, S.L. Yang, L. Ma, J. Li, and J. Hou, *J. Iron Steel Res. Int.* 23, 655 (2016).
12. C. Geng, T.C. Sun, Y.W. Ma, C.Y. Xu, and H.F. Yang, *J. Iron Steel Res. Int.* 24, 156 (2017).
13. Y.Q. Zhao, T.C. Sun, H.Y. Zhao, C.Y. Xu, and S.C. Wu, *ISIJ Int.* 59, 981 (2019).
14. L.S. Zhao, L.N. Wang, D.S. Chen, H.X. Zhao, Y.H. Liu, and T. Qi, *Trans. Nonferrous Met. Soc. China* 25, 1325 (2015).
15. T. Hu, X.W. Lv, C.G. Bai, and G.B. Qiu, *Int. J. Min. Met. Mater.* 21, 131 (2014).
16. H.Y. Sun, A.A. Adetoro, Z. Wang, F. Pan, and L. Li, *ISIJ Int.* 56, 936 (2016).
17. W. Li, G.Q. Fu, M.S. Chu, and M.Y. Zhu, *Steel Res. Int.* 88, 1600120 (2017).
18. W. Li, G.Q. Fu, M.S. Chu, and M.Y. Zhu, *Ironmak. Steelmak.* 44, 294 (2017).
19. J.B. Zhang, G.Y. Zhang, Q.S. Zhu, C. Lei, Z.H. Xie, and H.Z. Li, *Metall. Mater. Trans. B* 45, 914 (2014).
20. E. Park, and O. Ostrovski, *ISIJ Int.* 43, 1316 (2003).
21. F. Pan, Z. Du, M.J. Zhang, and H.Y. Sun, *ISIJ Int.* 57, 413 (2017).

22. H.Y. Sun, J.S. Wang, Y.H. Han, X.F. She, and Q.G. Xue, *Int. J. Miner. Process.* 125, 122 (2013).
23. E. Park, and O. Ostrovski, *ISIJ Int.* 44, 999 (2004).
24. Y.L. Sui, Y.F. Guo, T. Jiang, X.L. Xie, S. Wang, and F.Q. Zheng, *Int. J. Miner. Metall. Mater.* 24, 10 (2017).
25. Z.Y. Wang, J.L. Zhang, J.F. Ma, and K.X. Jiao, *ISIJ Int.* 57, 443 (2017).
26. L.Y. Yi, Z.C. Huang, T. Jiang, L.N. Wang, and T. Qi, *Powder Technol.* 269, 290 (2015).